Lawrence Berkeley National Laboratory
LBL Publications

Title
Mechanical Performance of Full-Scale Prototype Quadrupole Magnets for the sse

Permalink
https://escholarship.org/uc/item/20t8t106

Authors
Cortella, J M
Devred, A
Wandesforde, A

Publication Date
1992-08-01

Copyright Information
This work is made available under the terms of a Creative Commons Attribution License, available at https://creativecommons.org/licenses/by/4.0/

eScholarship.org Powered by the California Digital Library
University of California

LBL-32788
UC-414

Lawrence Berkeley Laboratory
UNIVERSITY OF CALIFORNIA

Accelerator & Fusion
Research Division

Presented at the Applied Superconductivity Conference,
Chicago, IL, August 23–29, 1992, and to be published
in the Proceedings

Mechanical Performance of Full-Scale Prototype Quadrupole Magnets for the SSC

J.M. Cortella, A. Devred, and A. Wandesforde

August 1992

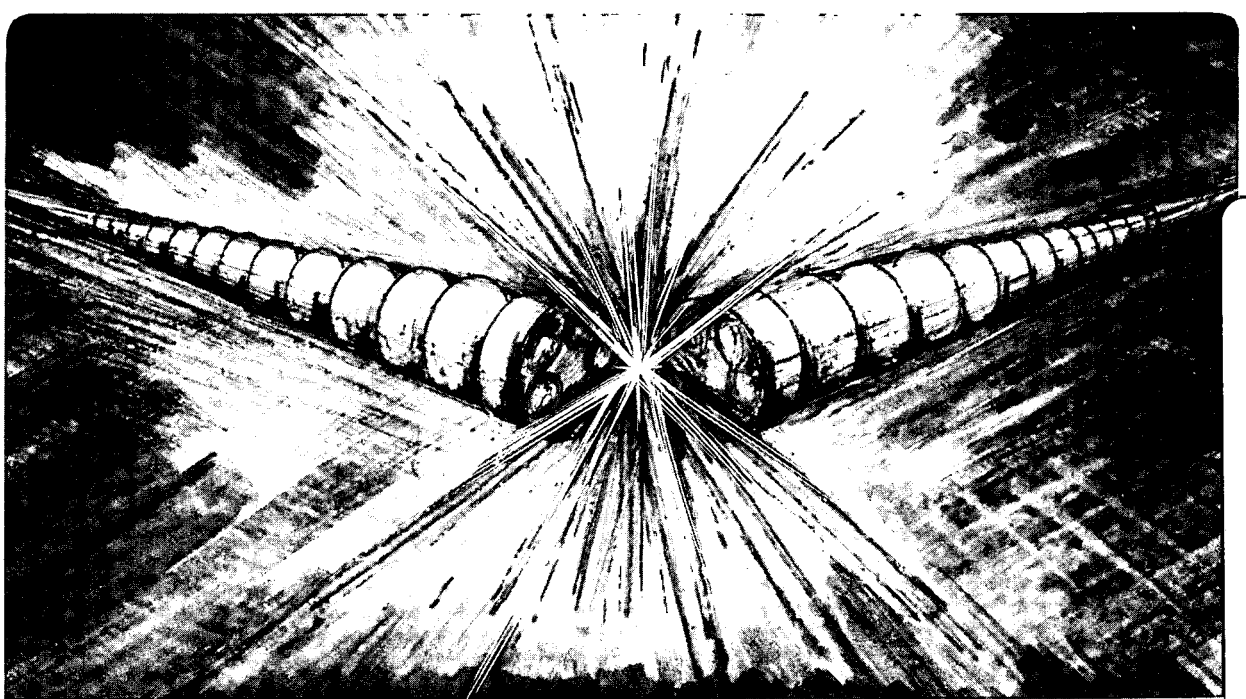

LBL-32788
Copy 2
Bldg. 50 Library.
for 4 weeks
Circulates
LOAN COPY

Prepared for the U.S. Department of Energy under Contract Number DE-AC03-76SF00098

DISCLAIMER

This document was prepared as an account of work sponsored by the United States Government. While this document is believed to contain correct information, neither the United States Government nor any agency thereof, nor the Regents of the University of California, nor any of their employees, makes any warranty, express or implied, or assumes any legal responsibility for the accuracy, completeness, or usefulness of any information, apparatus, product, or process disclosed, or represents that its use would not infringe privately owned rights. Reference herein to any specific commercial product, process, or service by its trade name, trademark, manufacturer, or otherwise, does not necessarily constitute or imply its endorsement, recommendation, or favoring by the United States Government or any agency thereof, or the Regents of the University of California. The views and opinions of authors expressed herein do not necessarily state or reflect those of the United States Government or any agency thereof or the Regents of the University of California.

LBL-32788
UC-414

Mechanical Performance of Full-Scale Prototype Quadrupole Magnets for the SSC

J.M. Cortella[1], A. Devred[2], and A. Wandesforde[1]

[1]Lawrence Berkeley Laboratory
University of California
Berkeley, CA 94720

[2]SSC Laboratory
2550 Beckleymeade Avenue
Dallas, TX 75237

August 1992

This work was supported by the Director, Office of Energy Research, Office of High Energy and Nuclear Physics, High Energy Physics Division, of the U.S. Department of Energy under Contract No. DE-AC03-76SF00098.

MECHANICAL PERFORMANCE OF FULL-SCALE PROTOTYPE QUADRUPOLE MAGNETS FOR THE SSC

J. M. Cortella[£], A. Devred[*], A. Wandesforde[£]

[£]Lawrence Berkeley Laboratory
1 Cyclotron Rd.
Berkeley, California 94720

[*]SSC Laboratory
2550 Beckleymeade Ave.
Dallas, Texas 75237

Abstract --Six 5-m-long prototype quadrupole magnets have been built and cold-tested at Lawrence Berkeley Laboratory for the Superconducting Super Collider. Each of the magnets contained instrumentation to monitor the mechanical performance of the magnets during assembly and cold-testing. In addition, the instrumentation was used along with physical measurements as aids during magnet assembly. Quantities measured include coil pressures during assembly, cooldown, and magnet energization; axial thermal contraction of the magnets during cooldown; and axial force transmitted to the magnet end-plates. For the most part, mechanical measurements have proven repeatable and agree well with analysis.

I. INTRODUCTION

The Superconducting Super Collider (SSC) is designed to use approximately 1700 quadrupoles in its main ring for beam focusing [1]. These magnets are five meters in length and have an aperture of 4 cm. A cross-section of the magnet is shown in Figure 1. In the past two years, six full-scale prototype magnets have been built and tested at Lawrence Berkeley Laboratory to evaluate the baseline design as well as various features implemented during the program that were seen as improvements.

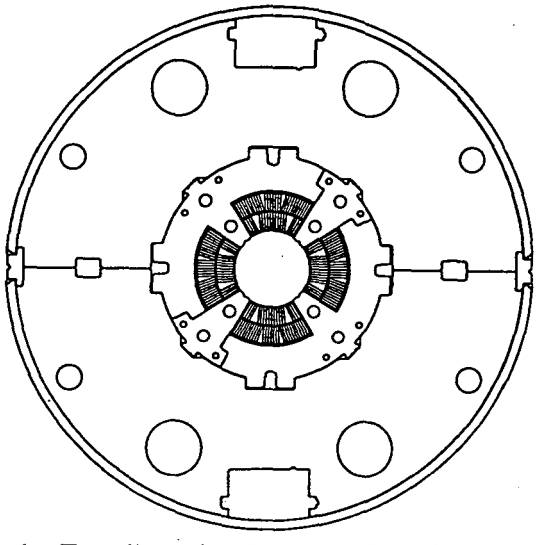

Fig. 1 - Two-dimensional cross-section of the SSC main ring quadrupole, showing all major components.

This paper will report on the mechanical behavior of the magnets, focusing on measurements made during cold-testing. The primary parameters studied were coil pressures, endloads, and axial expansion of the magnets. More details on the construction of the magnets as well as the quench performance and magnetic field quality can be found in another paper [2].

II. INSTRUMENTATION

Each of the six magnets was extensively instrumented to measure quench detection, thermal behavior, and mechanical performance, but this paper will focus only on the instrumentation used to measure the mechanical performance of the magnets. Strain-gauge collar packs were used to measure coil pressures, axial compression load cells were utilized to measure axial loads on the ends of the magnets, and strain-gauge extensometers were utilized to measure the axial expansion and contraction of the outer shell of the magnet.

A. Strain-Gauge Collar Packs

Each of the magnets in the series was equipped with two strain-gauge collar packs. These are specially designed collar packs containing a bending-beam load cell adjacent to the pole turn of each coil [3]. A total of eight of these transducers are located within each collar pack, four used to measure the pressures on the inner coils and four used to measure the pressures on the outer coils. The strain gauges in each of the transducers are wired in a full-bridge to provide temperature and magnetic field compensation. The two gauge packs comprise a total of sixteen load cells within each magnet, providing coil pressure data during assembly, cooldown, and magnet energization.

B. End Load Cells

Compression-type load cells are placed on the endplates of the magnet to measure the changes in end compression during cooldown and energization. Each of the six magnets was instrumented with these load cells. However, on magnet QCC401 only those load cells placed on the "lead end" (the end from which the current leads extend) of the magnet were monitored due to a limitation in the data acquisition system. There are four of these load cells placed on either end, equally spaced around the periphery of the endplates [4]. Axial loads from the magnets are transferred through the load cells and reacted by the outer shell. As are the gauge packs, these load cells are also instrumented with a full strain gauge bridge.

C. Axial Extensometers

On magnets QCC402, QCC403, and QCC405, the contraction and expansion of the shell during cooldown and warm-up were measured. This was done using a long, thin stainless steel ribbon welded to the outer shell of the magnet. The ribbon was welded at the two ends of the strip so that it would move with the magnet shell. It was instrumented with strain gauges to provide a measurement of the thermal strain over the length of the shell, independent of local variations in shell stress. When the strip was attached to the shell, it was given a pre-tensile load to prevent buckling should the shell shrink more than the strip.

III. ASSEMBLY MEASUREMENTS

A. Coil Size

Each of the eight coils in any magnet was measured after curing. The azimuthal size of the coils was measured at ten axial positions along the length of the magnet while under pressures ranging from zero to 70 MPa. The measurements showed both systematic deviations, which were traced to variations in the curing cavity size, and random deviations, which were largest in the end regions. At the beginning of the program, there was a fairly wide spread in the coil sizes. The coils used in magnet QCC401 had deviations within a single coil on the order of 150μm, and coil-to-coil deviations of as much as 125μm. However, as experience was gained, both variations within a single coil and coil-to-coil deviations were reduced to less than 50μm for the inner coils and 75μm for the outer coils.

Coil size deviations can effect the final collared coil pressure significantly. Deviations on the order of 25μm result in changes in pressure on the order of 6.2 MPa using aluminum collars and 8.9 MPa using steel collars [5]. Thus, even with the small variations in coil size mentioned above, it is possible to develop a fairly large spread of pressures within a magnet. Therefore, during the assembly of a magnet, coils are sorted to match coil sizes so that quadrant to quadrant deviations are a minimum.

B. Collaring

After sizing and sorting, the eight coils are assembled around a mandrel and collared with interlocking, laminated collars. During the collaring operation, the gauge packs are first utilized as a means to monitor the effects of different size shims placed at the pole during "test collaring." The purpose of the test collaring is to determine the proper shim size that will provide the coils with a sufficient amount of coil compression, such that the coils remain in compression throughout the operation of a magnet. The pole shim size is uniform throughout the magnet, although one size is often used for the inner coils and a second size for the outer coils.

In collaring a magnet, the target coil pressure is approximately 40 MPa when a magnet is at 4.3 K and at zero current. Thus, in selecting a pressure at which to collar a magnet, it is necessary to compensate for any thermal contraction differences and loss in load due to creep of components. In addition, during the collaring operation, a hydraulic press is used to secure and compact the collars and coils so that the locking keys can be inserted without having to overcome large amounts of friction. The pressures on the coils during this operation are higher than the final collared pressure. Shown in Table 1 are the average peak stresses seen by the inner coils of each magnet, the final collared pressures, and the pressures just prior to the initial cooldown, showing the effects of creep. Cooldown effects will be discussed extensively in the next section.

Table 1 - Average Inner Coil Pressures During the Assembly of the QCC Quadrupoles (MPa)

	Peak Pressure	After Collaring	Prior to Cooldown
QCC401	--	39.1	36.8
QCC402	48.4	36.7	33.7
QCC403	54.1	41.7	39.8
QCC404	95.4	80.8	108.3
QCC405	120.2	75.6	68.2
QCC406	86.3	49.9	46.2

A number of salient points of Table 1 should be mentioned. First, the last three magnets were collared at higher pressures because they were constructed with stainless steel collars, which would result in thermal contraction changes greater than the first three magnets, as discussed in the next section. Also, for magnet QCC404 the pressure prior to cooldown is higher than the final collared pressure because this magnet was assembled with an interference between the collars and surrounding iron yoke, providing additional mechanical support. The increase represents the influence of the yoke at room temperature. Also, pressures greater than 80 MPa may not be very accurate, as the load cells are only calibrated to 80 MPa.

IV. COOLDOWN

During the cooldown of a magnet, differences in the thermal contraction properties of the magnet components lead to changes in the coil azimuthal stress as well as the axial loading. In this section, a summary of the cooldown changes in the coil pressures and endloads for each of the magnets is presented.

A. Prediction of Cooldown Changes in Coil Pressure

If the magnet is considered a uniform two-dimensional structure, it should be a simple matter to predict the changes in stress due to thermal contraction differences. For reference, only magnet QCC404 was designed to be supported by the yoke and outer shell. Also, a key design parameter of the magnets is the collar material. The first three magnets in the series used aluminum collars; the last three used Nitronic 40 stainless steel [2]. For the key materials used in this study, the thermal contraction coefficients between room temperature and liquid helium temperature are as follows [5]: aluminum, 4.0 mm/m; Nitronic 40 stainless steel, 3.0 mm/m; low-carbon steel, 2.0 mm/m; NbTi superconducting coil, 4.3 mm/m.

In addition to the differences in thermal expansion properties, there is another factor that must be considered in the prediction of a change in coil pre-compression. This being the fact that the conductor used in the SSC magnets has a distinct non-linear stress-strain behavior. This property complicates the prediction process considerably. The stress-strain behavior is very nearly parabolic, with an increasing modulus at higher stress levels. By fitting the curve with a parabolic equation, it is possible to analyze the effect this behavior has on the cooldown changes. An approximate relation for the stress-strain behavior of the coils is, from [6],

$$\sigma = A\varepsilon^2 + B\varepsilon + C \qquad (1)$$

with $A = 1.1 \times 10^6$ MPa, $B = -3400$ MPa, and $C = 8.0$ MPa.

The details of the prediction process can be found in [6], but the procedure essentially involves the computation of thermal contraction induced dimension changes in the coils, collars, and other major components. Then, using the length changes, one can compute the strain changes and resulting stress changes. After a bit of algebra and incorporating Eq. (1), the stress change from warm, σ_W, to cold, σ_C, is

$$\Delta\sigma = \sigma_W - \sigma_C = 2A\Delta\varepsilon^2 + (4A\varepsilon_W + B)\Delta\varepsilon. \qquad (2)$$

The above relation shows that the change in stress depends on the room temperature value of the strain. Thus, the greater the initial compression, the greater the pressure change during cooldown. In Eq. (2), the warm strain value is determined from the room temperature pressure value and Eq. (1).

B. Summary of Measured Cooldown Coil Pressure Changes

Plotted in Figure 2 are the predicted changes in stress for the quadrupole magnets for the different types of collar materials used, as well as the actual average cooldown losses from each of the six magnets tested. Each data point represents an average of the measurements from the four coils within a gauge pack. The test data and the analytical predictions both show that little change is expected in coil compression using aluminum collars; this because the coils and aluminum have similar thermal contraction properties. Thus, the use of aluminum collars allows one to assemble a magnet at lower initial pressures than a steel collared magnet, but still retain sufficient coil compression when cold.

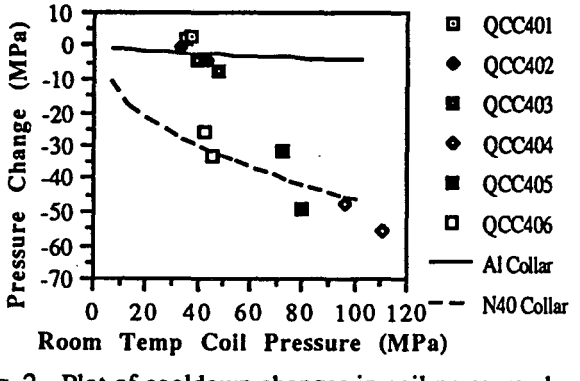

Fig. 2 - Plot of cooldown changes in coil pressure along with predicted relations for each of the six SSC quadrupoles tested.

One further aspect of the data in Fig. 2 needs to be considered as well. As mentioned earlier, magnet QCC404 utilized the yoke for support. It was built with a nominal interference of 100μm between the collars and the yoke. As the steel collars shrink away from the yoke, one expects an added loss in compression as a result of the release of stored elastic energy. This should result in greater cooldown changes than the non-supported magnets. However, as shown in Fig. 2, QCC404 seems to behave the same as the other steel-collared magnets. The reason for this apparent discrepancy is not fully understood. More data on yoke-supported magnets would be necessary to make any conclusions regarding the behavior of yoke-supported magnets.

C. Prediction of Endload Change During Cooldown

The primary means of end support was the use of a one-inch-thick steel endplate butted up against the end of the coils. However, in some magnets, additional support was used. In magnets QCC402, QCC404, QCC405, and QCC406 an additional ring was clamped around the coils 15 cm away from either end. The ring clamp was then bolted to the last yoke block, which is physically mated to the shell via a large frictional force as a result of weld shrinkage. Thus, the coils, yoke, and shells are all tied together; the idea being that they would all move together during any axial expansion or contraction.

The manner in which a magnet was supported axially had a pronounced effect on the change in axial load during cooldown. In the magnets with the bolted-ring clamp, the changes in endload observed are a result of changes within the end region of the magnet only, since the straight section of the magnet is locked to the shell. The changes observed are a function of the thermal contraction differences of the aluminum end clamp and the stainless steel shell as well as the relative stiffness of magnet components in the end region. These length contractions along with calculated stiffnesses can provide a prediction for the cooldown loss following Hooke's Law. The calculated stiffness of the end region, with the aluminum end clamp and the coil end acting as two springs in parallel with the endplate acting as a spring in series, would be

$$k_{eq} = \frac{k_1(k_2 + k_3)}{k_1 + k_2 + k_3} \qquad (3)$$

where k_1 = stiffness of endplate = 1.2×10^5 kN/m from [7]

k_2 = stiffness of coil end

$$= \left(\frac{AE}{L}\right)_{end} = 3.4 \times 10^5 \text{ kN/m}$$

k_3 = stiffness of aluminum end clamp

$$= \left(\frac{AE}{L}\right)_{alum} = 5.1 \times 10^5 \text{ kN/m}.$$

In the above,

A = the area of the coil end or aluminum clamp (m^2)

E = the elastic modulus of the coil end, assumed to be dominated by the G-10 end spacers, or aluminum end clamp (MPa)

L = the length of the region between the endplate and the bolted-on ring clamp (15cm).

This results in an equivalent stiffness of 1.1 x 10^5 kN/m, which agrees fairly well with an experimentally measured value of 9.2 x 10^4 kN/m. Based on a change in length determined by the thermal contraction difference between the aluminum endclamp and the stainless steel shell during cooldown (1 mm/m), the loss in axial compression in the last 15 cm should be approximately

$$F = k_{eq}\Delta x = 1.1 \times 10^5 \text{ kN/m}[(.001\text{m/m})]0.15\text{m} = 16.5 \text{ kN}.$$

D. Summary of Measured Endload Changes During Cooldown

Listed in Table 2 is a summary of the endload changes during cooldown for each of the six magnets in this study. Although the scatter in the data is fairly large, average load changes agree well with prediction for the four magnets that used the end clamp, locking the straight section of the magnet to the shell.

Table 2 - Changes in Endplate Load for Six SSC Quadrupoles During Cooldown (kN)

	Lead Endplate	Return Endplate
QCC401	5.0	-
QCC402	14.7	14.6
QCC403	51.7	50.1
QCC404	11.6	14.7
QCC405	9.2	24.1
QCC406	21.4	19.3

The load change in QCC401 is low by comparison. Magnet QCC401 did not utilize a bolted-ring end clamp, and therefore, the region which was affected by thermal contraction differences included a significant portion of the straight section of the coils. In this situation, the end region is much less stiff, and the differences between the thermal contraction of the stainless steel shell and the aluminum end clamp have little effect in changing the load.

The endload change in QCC403 is notably high. This is a result of a modification in design compared to the other magnets. In all magnets except QCC403, the endplate contacted solely the end of the coils and not the much larger diameter aluminum end clamp surrounding the coil ends. However, in magnet QCC403 additional shims were placed between the endplate and the large aluminum end clamp, distributing the load over a much wider area. This effectively increased the stiffness of the end region by a factor of three, and the load changes during cooldown seem to be a response to this design change.

E. Axial Expansion

The axial extensometer strips which were placed on the outer diameter of the shell were made of stainless steel, as was the shell itself. Therefore, any apparent strain measured on the gauges would be due to *differences* in thermal contraction between stainless steel strip and the shell. The shell has a greater coefficient of thermal expansion than does the yoke around which it is welded. Therefore, as the shell shrinks around the yoke, azimuthal stress will increase. This increase in azimuthal stress translates to an increase in the axial strain as dictated by Poisson's ratio, which is 0.3 for steels.

In each of the magnets on which the axial expansion strips were used, an apparent change in strain of approximately 0.2 millistrain was measured. If the shell were free to expand and contract longitudinally, the axial strain that would be expected would be simply Poisson's ratio multiplied by the azimuthal strain. Given that the difference in thermal expansion between the stainless steel shell and the iron yoke from room temperature to liquid helium is 0.9mm/m, the expected axial strain would be 0.27 millistrain.

A possible explanation for the difference between the 0.2 value measured and the theoretical value of 0.27 is because the shell is not free to contract axially. The iron yoke is placed on the magnet in eighteen-inch-long sections known as yoke packs. These packs are placed on the magnet by hand, and small gaps are left between each pair of yoke blocks. As the magnet cools, these blocks are pulled together by the shell, and the gaps eventually close. Once the gaps are closed, the shell is no longer free to contract; it behaves as the yoke blocks do. Thus, the overall axial contraction is less than what it would be had the shell been completely free to contract.

V. ENERGIZATION

A. Prediction of Coil Unloading During Energization

During energization of a magnet, the Lorentz forces acting upon a coil result in a redistribution of stress within the coils. These forces are proportional to the product of the magnetic field and the current in the coils. In addition, the field is proportional to the current as well. Therefore, it follows that the Lorentz forces are proportional to the square of the current. Thus, all plots and data comparisons will discuss the behavior of the energization loads as a function of current squared.

Analytical computations used to predict the degree of the coil unloading during energization give a value of approximately 0.21MPa/kA^2 for both the inner and outer coil [8]. These models use a constant elastic modulus to represent the behavior of the coils, and computations provide an "energization response" which is independent of initial values. Therefore, at the operating current of the SSC, 6500A, the coils should lose approximately 8.9 MPa.

B. Summary of Coil Pressure Changes During Energization

Shown in Figure 3 is a typical trace of the inner coil pressures during the energization of a magnet as a function of the current squared. The data is from magnet QCC404. The data represent the coil pressures from each of the four quadrants in the gauge pack nearest the end of the magnet with the current leads. The labels in the legend represent the individual load cell identification numbers, with the number corresponding to the respective quadrant.

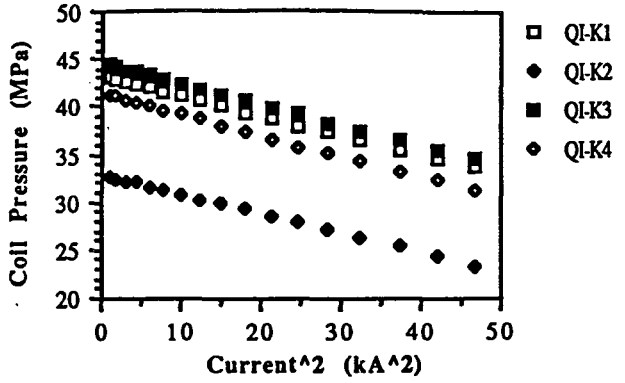

Fig. 3 - Trace of inner coil pressures during the energization of magnet QCC404 at 4K.

As with the coil pressure changes during cooldown, the changes during energization also were a function of the initial pressure level. The higher the initial pressure, the greater the magnitude of the slope. For the traces shown, the slopes vary from 0.25 MPa/kA^2 for the trace starting at 33 MPa to 0.35 MPa/kA^2 for the curve with an initial value of 45 MPa.

The dependence of the slope on the initial pressure is again a product of the non-linear elastic properties of the conductor, as discussed earlier. If the slopes of each of the individual load cell signals are plotted as a function of the initial pressure on the magnet, then a definite relation develops. Figure 4 presents such data. It displays the average of the inner coil slopes from each gauge pack for each of the six magnets tested. Therefore, the analytical prediction developed with finite elements using linear elastic coil properties mentioned earlier is not very accurate. Actual values may differ from the predicted value by as much as a factor of two.

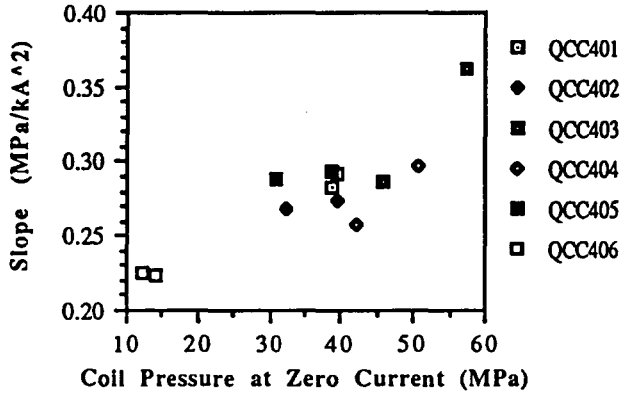

Fig. 4 - Dependence of energization response of the inner coils on initial pressure level.

In addition, there are other influences that affect the changes during energization. It was discovered that a magnet responds differently on its first energization than it does during subsequent energizations. Shown in Figure 5 is a trace of two load cells from the first energization of magnet QCC406. The magnet was cycled between 0A and 5000A three times and then ramped to quench. The coil pressures do not return to their original zero current values after the initial energization to 5000A. In addition, there is a decrease in the slope of the traces, all of which indicates that the coils have been compacted into a slightly tighter, stiffer package after being subjected to the Lorentz loading. These changes in the slopes and shifting of zero current pressure levels indicate that the Lorentz load tends to reposition the coils into a "favorable" position.

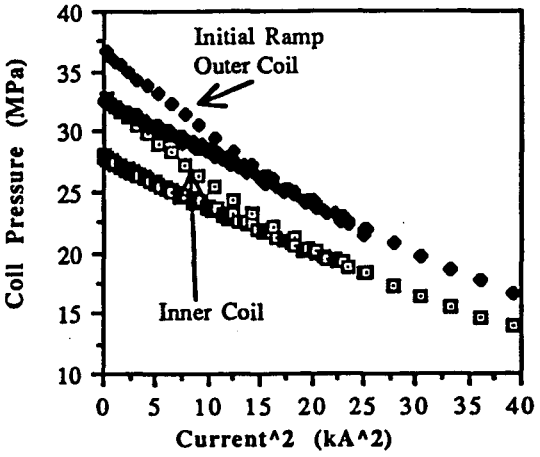

Fig. 5 - Comparison of initial and subsequent rampings of a magnet, showing changes in coil pressure. Data is from first training of magnet QCC406.

C. Effects of a Thermal Cycle on Coil Pressures

The changes in energization response of the coils are obviously more than a by-product of the materials properties of the conductor or other components, since the response changes once the magnet reaches a new current level. It appears that there is a frictional force that locks the coil in a new position once it has been energized beyond a certain force level. This locking into place may be a key to training. There is a stable position within the magnet that allows it to reach a plateau current comparable to the critical current. Unfortunately, in order for the conductor to move into this favorable position, it must overcome friction, resulting in small amounts of heat generation which force the conductor into a normal state, and quenching occurs. Each of the quadrupoles tested have had a significant number of training quenches, although the number has decreased with the later magnets [2].

An important question is whether or not the changes in mechanical behavior that took place during the initial training remain once a magnet has been warmed to room temperature and re-cooled. If the behavior shown in Fig. 5 does not manifest itself during the second training cycle, then one might say that the magnet "remembered" its initial training, and its quench performance should improve. Unfortunately, subsequent cold-testing of magnets have always shown very repeatable behavior. Coil pressure traces versus current squared from the first quench after a magnet has been warmed and cooled a second time are essentially identical to the original tests.

Other evidence of the magnets' inability to remember its training is illustrated in "history" plots of the coil pressure. They show that the sums of the coil pressure changes during

cooldown and the zero current shifts that take place during cold-testing are equal to the coil pressure changes during warm-up. Figure 6 plots the history of the average coil pressures within each gauge pack of magnet QCC403. The labels on the horizontal axis refer to subsequent steps in the testing of a magnet, from just prior to the initial cooldown to the final room temperature reading. The "cold" label refers to the coil pressure taken once the magnet has reached liquid helium temperature but prior to any energization of a magnet. The "plateau" label refers to coil pressures at zero current taken once a magnet has been repeatedly quenched. The figure shows that the magnet "forgets" its training. That is, after a thermal cycle, the magnet returns to its initial state, and when cooled a second time, it returns to its pre-energized state.

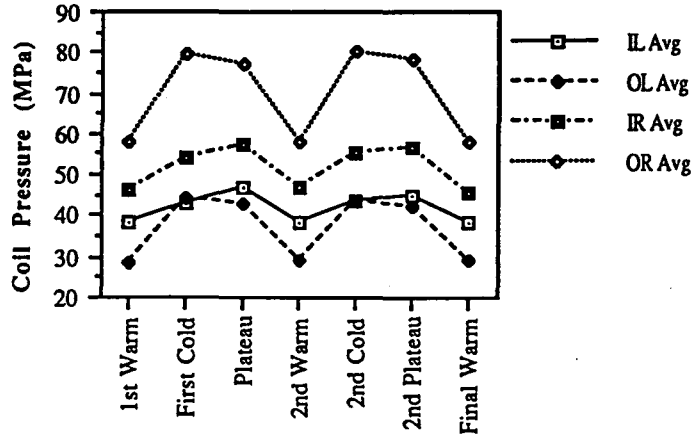

Fig. 6 - History of inner coil load cells during various phases of cold-testing of magnet QCC403. In the legend, I represents inner coil; O, outer coil; L, lead end pack; and R, return end pack.

D. Endload Behavior During Energization

Four of the six magnets tested used an end design that locked all but the last 15 cm of the coils to the shell. Therefore, the endload changes during energization are primarily a product of the relative motions in the very end region of the magnets, the last 15 cm or so between the endplates and the bolted-ring clamp used in all magnets except QCC401 and QCC403. The total axial Lorentz load has been calculated to be 24.5 kN [8], pulling the ends of the coils outward. Table 3 lists the slopes of the endload versus current squared traces and the percentage of predicted. The difference in the measured and the predicted values is due to the stiffness of the coils and the mechanisms used to transfer load directly to the outside skin.

Table 3 - Endload Responses of QCC Quadrupoles

	Response (kN/kA^2)	% of Total Predicted
QCC401	0.28	48.0
QCC402	0.068	11.7
QCC403	0.258	44.5
QCC404	0.036	6.2
QCC405	0.034	5.8
QCC406	0.027	4.7

The effect of the bolted-ring end clamp is clearly illustrated, with as little as 5% of the axial Lorentz load being transferred to the endplates. As mentioned earlier, these rings were employed so that the collared coil, yoke blocks and skin would all move together in the axial direction. The measured responses are largely a result of motions only in the very end region of the coils.

However, with magnets QCC401 and QCC403, the only way axial Lorentz load could be transferred to the shell without appearing at the endplate was through collar-yoke friction. Since the yoke was not intended to support the collars in these magnets, the response values are considerably higher than for other magnets that used the bolted-on end clamp.

VI. SUMMARY

The six prototype SSC main ring quadrupoles have shown repeatable mechanical performance. Instruments developed to monitor mechanical behavior have provided information on the behavior of the magnets during assembly, cooldown, and energization. The instruments developed were used to monitor coil pressures, endloads, and axial expansion of the magnets. During assembly, the instrumentation was a useful assembly aid. Measurements have shown that the magnets' behavior during cooldown is as predicted, but depends highly on the non-linear material properties of the conductor. From cold-testing, the primary result from the measurements is the demonstration of the inability of these magnets to "remember" their initial training. It has been demonstrated that Lorentz loading of a magnet changes the mechanical behavior of the magnets. But, upon having been warmed to room temperature, cooled, and then retested, their mechanical behavior is nearly identical to that during the initial energization. Axial contraction data and endload behavior are consistent with design features of each magnet.

REFERENCES

[1] J.R. Sanford, D.M. Matthews, eds., "Site Specific Conceptual Design for the Superconducting Super Collider," SSCL-SR-1056, July, 1990.

[2] A. Lietzke, C. E. Taylor, et al "Construction and Test Results of 40 mm Bore 5m Long Quadrupole Magnets for the SSC," Paper LN-4, In these proceedings.

[3] A. Wandesforde, "Load Cell Pack for LBL SSC Quadrupole Prototypes," LBL-DWG-23F6806. 1990.

[4] J.M. Cortella, "Axial Load Measurements on Superconducting Magnets," SC-MAG-357, 1991.

[5] J.M. Cortella, "Preliminary Study of the Mechanical Performance of SSC Quadrupole Magnets," LBL Report SC-MAG-368, 1992.

[6] A. Devred, et al, "About the Mechanics of SSC Dipole Magnet Prototypes." AIP Conference Proceedings, Vol. 249 (2), 1992, pp. 1309-1374.

[7] Roark and Young. *Formulas for Stress and Strain*, 5th ed. McGraw-Hill, New York, 1975.

[8] D. Dell'Orco, "Finite Element Analysis of the QC Quadrupole for the SSC," LBL Report SSC-MAG-260.

[9] S. Caspi, Private communication.

LAWRENCE BERKELEY LABORATORY
UNIVERSITY OF CALIFORNIA
TECHNICAL INFORMATION DEPARTMENT
BERKELEY, CALIFORNIA 94720